10g

MTL TR 90-54

AD

FORMATION OF CONTROLLED ADIABATIC SHEAR BANDS IN AISI 4340 HIGH STRENGTH STEEL

JOHN H. BEATTY
U.S. ARMY MATERIALS TECHNOLOGY LABORATORY
METALS RESEARCH BRANCH

LOTHAR W. MEYER
FRAUNHOFER-INSTUT FUR ANGEWANDTE MATERIALFORSCHUNG (IFAM)
D-287, BREMEN 77, WEST GERMANY

MARC A. MEYERS and SIA NEMAT-NASSER
UNIVERSITY OF CALIFORNIA, SAN DIEGO
La JOLLA, CA 92093

November 1990

US ARMY
LABORATORY COMMAND
MATERIALS TECHNOLOGY LABORATORY

U.S. ARMY MATERIALS TECHNOLOGY LABORATORY
Watertown, Massachusetts 02172-0001

CONTENTS

INTRODUCTION

Adiabatic shear bands have been previously studied because of their importance both in metal working operations (such as turning, reaming, punching, and forging) and in other processes at high strain rates (such as armor and projectile failure, and explosive forming). An adiabatic shear band consists of a narrow region of concentrated strain where the strain rate is sufficient to preclude significant heat transfer away from the sheared region. The material within the band experiences both significant increases in temperature and a large accumulated strain. In steels, two types of adiabatic bands have been distinguished using optical metallography: the "transformed" type which etches white using nital, and the "deformed" type which etches dark. The term "transformed" was originally used to suggest that the phase transformation from α (ferrite) to γ (austenite) had taken place within the band during shearing, though many investigations have failed to provide conclusive evidence that a phase transformation is necessary to produce a white etching or "transformed" band. However, because of common usage, this notation will be adhered to until conclusive evidence to the contrary is found.

This research program is aimed at studying the microstructural and mechanistic evolution of adiabatic shear bands in high-strength steels. Specifically, the deformation processes and their relation to controlled microstructural constituents (carbides) have been examined through the use of optical microscopy, scanning electron microscopy (SEM) and transmission electron microscopy (TEM). This paper examines the applicability of our testing techniques to study initiation mechanisms and presents some preliminary observations.

EXPERIMENTAL PROCEDURE

In order to study the effects of microstructure on adiabatic shear initiation, both the microstructure and the shear deformation must be controlled. The microstructures of VAR 4340 steel used in the present study have been previously characterized by Cowie et al.[1,2] The controlled variable is the size and distribution of the carbides present in the tempered martensitic microstructure without changing the material's hardness (Rc52). This is accomplished by using different normalizing temperatures (845°C, 925°C, 1010°C, or 1090°C for two hours) to produce each microstructure. The range of possible grain refining carbide phases are redissolved and/or coarsened to differing degrees at each normalizing temperature. These carbide distributions do not change during the final, short duration austenitization treatment at 845°C for 15 minutes (oil quenched). This is followed by a 200°C temper for two hours. This produces microstructures with constant prior austenite grain size (ASTM 12) and hardness but with different carbide distributions.

The controlled initiation and propagation of shear bands occurred during split Hopkinson compression bar testing using the experimental technique of Meyer et al.[3,4] with a hat-shaped specimen. The experimental arrangement, schematic stress history, and sample geometry are shown in Figure 1. Using this type of test, it is possible to study microstructure changes just before and after the initiation of the bands. A 19 mm (0.750 in.) diameter Hopkinson bar was utilized, with a 152 mm (6 in.) long striker traveling at a velocity of 18.3 m/s. Shear strain rates from 10^3 to 3×10^5 s^{-1} are obtained.

1. COWIE, J. G. *The Influence of Second Phase Dispersions on Shear Instability and Fracture Toughness of Ultrahigh Strength 4340 Steel.* U.S. Government Report, U.S. Army Materials Technology Laboratory, Watertown, MA, MTL TR 89-20, March 1989.
2. AZRIN, M., COWIE, J. G., and OLSON, G. B. *Shear Instability Mechanisms in High Hardness Steel.* U.S. Government Report, U.S. Army Materials Technology Laboratory, Watertown, MA, MTL TR 87-2, January 1987.
3. HARTMAN, K. H., KUNZE, H. D., and MEYER, L. W. *Metallurgical Effects on Impact Loaded Materials.* in Shock Waves and High-Strain-Rate Phenomena in Metals, M. A. Meyers and L. E. Murr, Eds., Plenum Press, New York, 1981.
4. MEYER, L. W., and MANWARING, S. *Critical Adiabatic Shear Strength of Low Alloyed Steel Under Compressive Loading.* in Metallurgical Application of Shock-Wave and High-Strain-Rate Phenomena, L. E. Murr, K. P. Staudhammer, M. A. Meyers, eds., Marcel Dekker, Inc., New York, 1986.

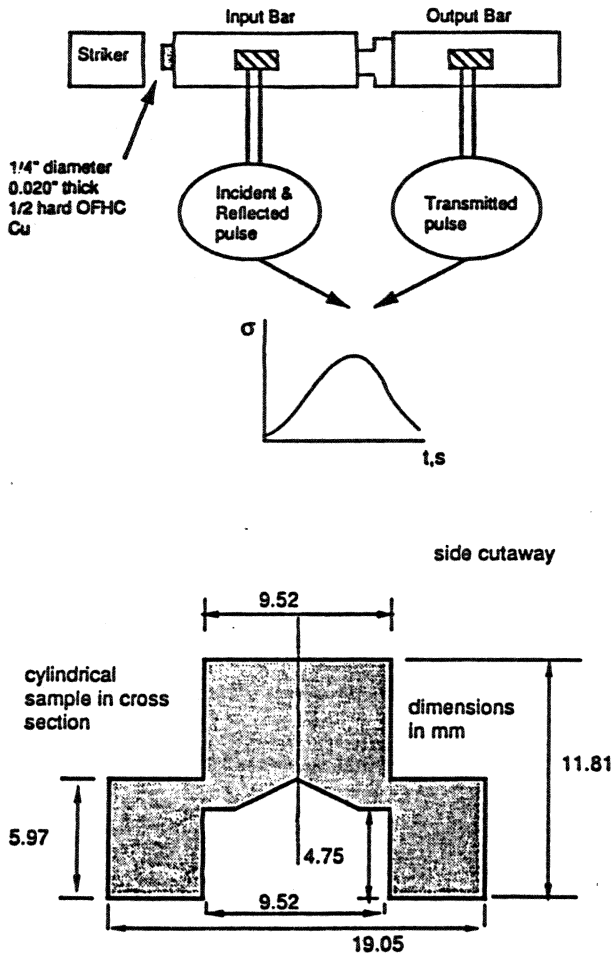

Figure 1. Hopkinson bar with experimental configuration and schematic stress history (a) and "hat" specimen geometry (b) developed by Meyer et al. (see References 3,4).

Initial tests using this apparatus showed that ringing effects altered results during sample failure. To eliminate this problem, a small copper disc (6.35 mm diameter and 0.5 mm thickness) is placed in between the striker bar and the input bar. This creates a trapezoidal (ramped) shaped input wave and eliminates the ringing. Pulse shaping of this kind has been utilized for dynamic testing of ceramics.[5] Stress and displacement measurements were calculated from the transmitted and reflected elastic waves in the bars. In order to control the degree of deformation introduced, stop rings are placed around the small cylinder of the

5. RAVICHANDRAN, G., and NEMAT-NASSER, S. *Micromechanics of Dynamic Fracturing of Ceramic Composites: Experiments and Observations.* Proceedings of the ICF-7, Texas, March 20-24, 1989, Advances in Fracture Research, v. 1, 1989, p. 4-48.

"hat". With a range of stop ring lengths, it is possible to halt the shearing process at different stages of plastic deformation. From these interrupted samples, metallographic, SEM, and TEM specimens were produced enabling the observation of microstructure-deformation interactions and the development of bands.

TEM samples of the sheared regions were made by mechanically thinning the material to a thickness of less than 0.125 mm. Three millimeter discs were abrasively cut from the thinned material using a slurry disc cutter. The foils were electropolished in a 5% perchloric, 95% methanol solution at -20°C and 50 V. The shear band region polished preferentially but produced insufficient electron transparent regions. Ion milling at 15° impact angle and 4 kV was used to further thin the specimens for TEM examination. Both a 300 kV Philips CM-30 and a JEOL 200 CX electron microscope were used.

RESULTS

Shear bands are easily produced in the hat specimens. Figures 2a and 2b show shear band development using optical microscopy in typical samples. The shear bands etch white in nital, typical of the "transformed" band type. Figure 2b shows the deformation zone before the "transformation" bands have formed in a sample with interrupted deformation.

Some specimens undergoing larger displacements with full shear band deformation often exhibited cracks along the shear bands; these cracks along shear bands are common. Since their orientation with the original imposed shearing direction (see Figure 3) would *close* the cracks and not open them, it is concluded that the cracks must have formed after the removal of the imposed shear stresses. It is also indicative of the increased hardness usually associated with the shear band material after testing.

A typical stress-time diagram obtained by these tests is shown in Figure 4a, along with the velocity of the input bar in Figure 4b; this sample was normalized at 845°C. After the sample reached its ultimate shearing strength (instability stress), the load drops until the stopper ring is impacted at about 275 μs. Note also that the velocity of the input bar remains smoothly increasing at a moderate rate (from 4.4 m/s to 5.6 m/s) throughout the regime of interest (260 μs to 265 μs), during which the sample transitions from elastic deformation to stable plastic flow to unstable plastic flow. An average displacement rate of 5.1 m/s was used to calculate the average strain rate of these tests.

Using the above mentioned displacement rate and the uniform deformation zone width estimated from Figure 2b (50 μm), a strain rate before shear band formation of $\dot{\gamma} = 1.01 \times 10^5\ s^{-1}$ can be derived. The strain rate after shear band formation can be approximated if one assumes that only the material within the shear band continues to deform and remains at constant width; however, we have observed some widening of shear bands as shearing has progressed. Using a shear band width of 9 μm (see Figure 2b), a strain rate of $\dot{\gamma} = 5.64 \times 10^5\ s^{-1}$ in the shear band is calculated.

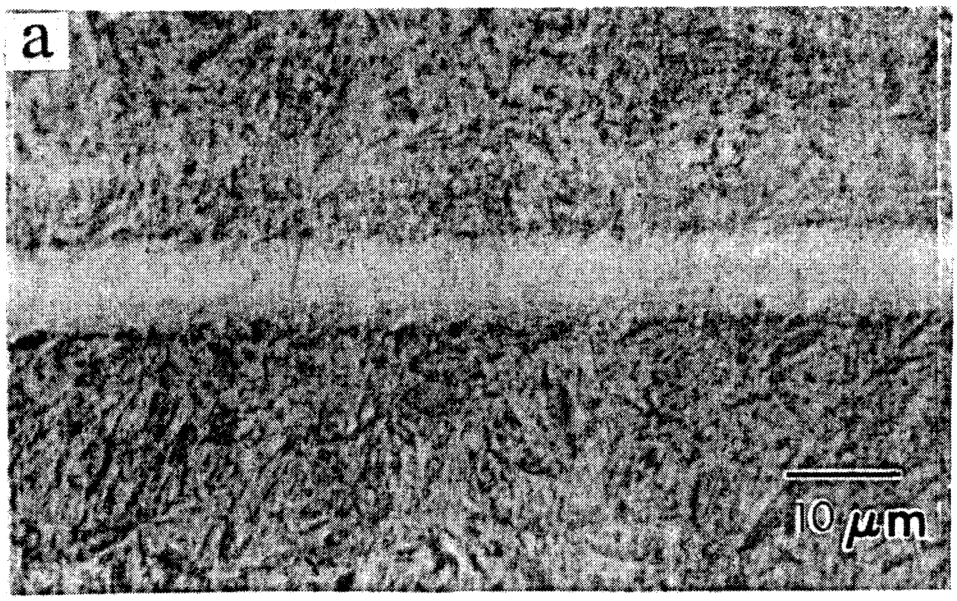

Figure 2a. Optical micrographs of shear bands produced using this sample geometry. Samples were from the microstructure normalized at 845°C.

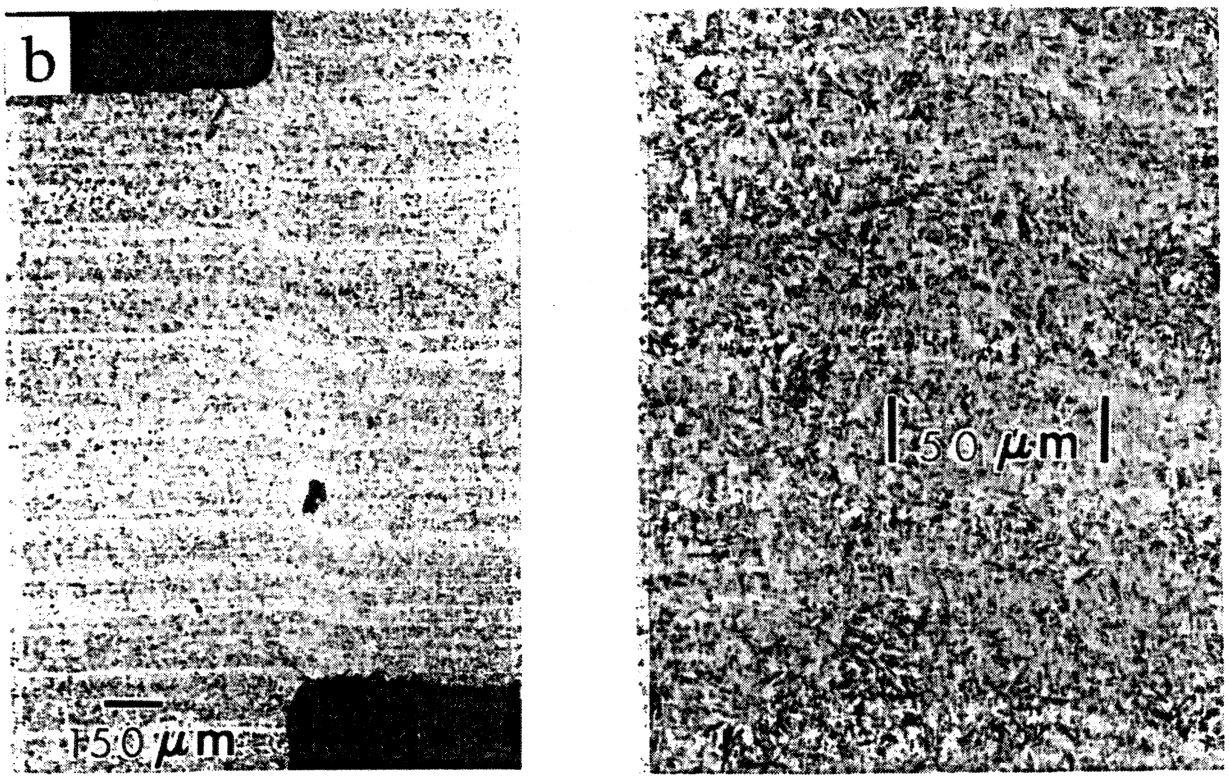

Figure 2b. Illustrates a sample "stopped" prior to the development of a "transformed" band.

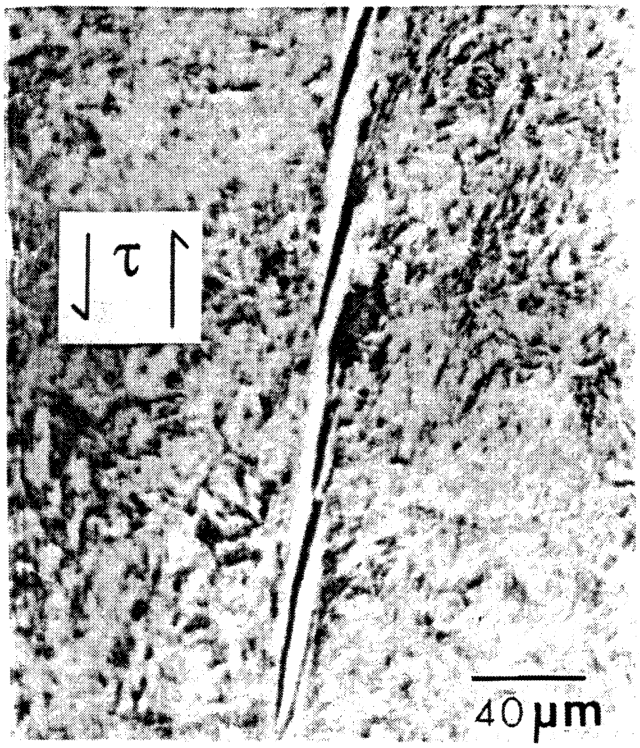

Figure 3. Tension cracks produced in the specimens upon unloading. Original loading direction is noted. Normalized at 925°C.

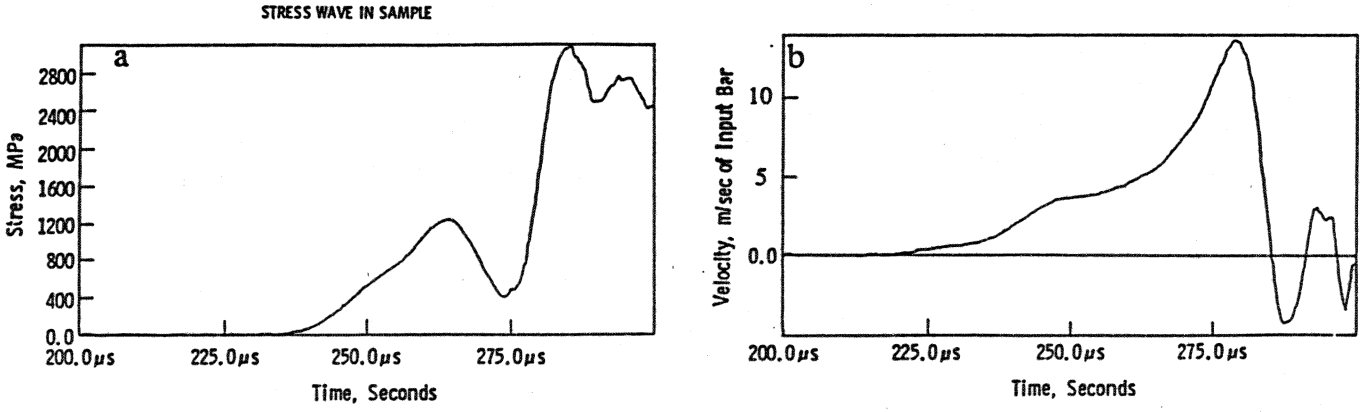

Figure 4. Typical (a) shear stress/time and (b) input bar velocity/time curves.

From the stress-time and velocity-time curves, a stress displacement curve may be generated. Both a typical engineering shear stress and the corresponding true shear stress versus displacement curve are shown in Figure 5. The true stress values are valid only up to the instability stress. These curves have a large linear region, and the stresses fall smoothly after instability. Earlier studies by Meyer et al.[3,4] displayed steeper drops after the maximum shear stresses were reached for a low alloy steel (VHN 480) and a CrMoV steel of medium strength (σ_{ys} = 1300 MPa at $\dot{\gamma} = 10^{-4}$ s^{-1}).

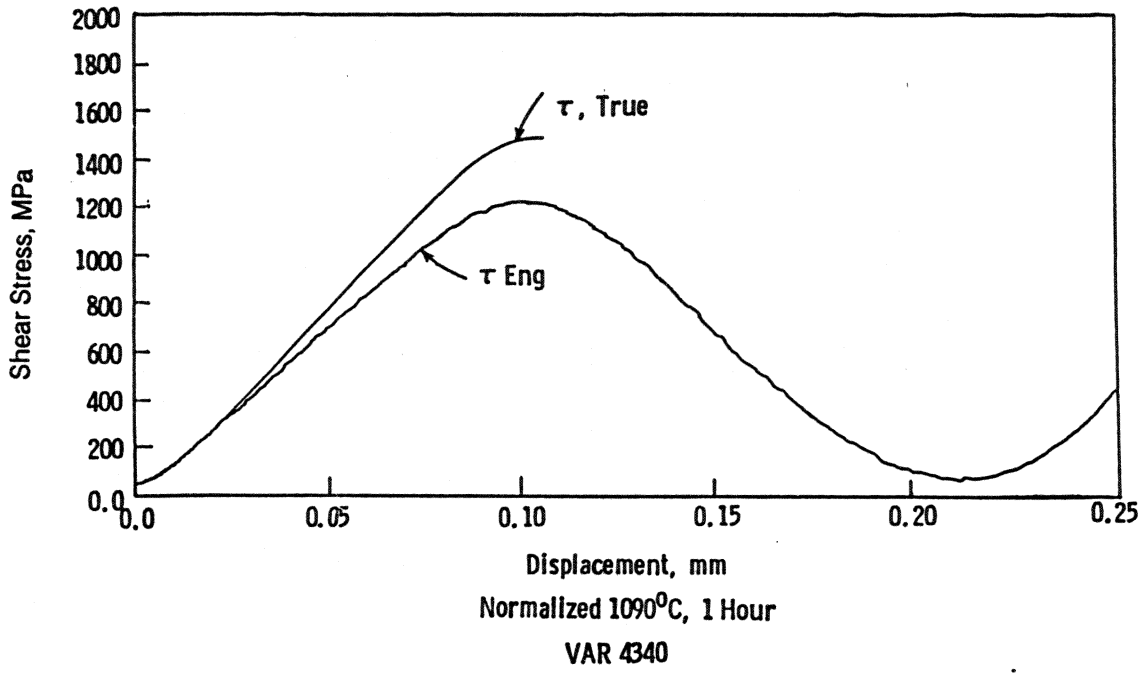

Figure 5. Typical engineering shear stress-displacement and true shear stress-displacement curves (true stress curve is only accurate up to the point of instability).

Figure 6 is a plot of the maximum engineering and true stresses reached as a function of normalizing temperature. Virtually no change is apparent as the maximum shear stress attained was independent of the four microstructures tested. The same microstructures were previously studied[1,2] at low strain rates in pure shear, and here, too, no effect on the instability stress was found. However, significant differences between the microstructures were noted when energy absorption was considered. Figure 7 plots the energy absorbed before instability (E_i) versus normalizing temperature relationship for a strain rate of $\dot{\gamma} = 10^5$ s^{-1}; note the energy peak for the 925°C normalizing temperature.

Electron microscopy was used to examine the transition between the matrix and the shear bands. Figure 8a is a SEM micrograph of a shear band formed in the microstructure normalized at 925°C. Figure 8b shows this band near its tip. Note the alignment of the martensite laths with the shearing direction along the band edges and the absence of any resolvable grain structure within the band at this magnification. "Flow" lines can be detected parallel to the shear direction within the band. Figure 9a shows a portion of the shear band region

examined in the TEM. The microstructure appears mottled, unlike normal martensite, and the presence of many moiré fringes are noted. A Selected Area Diffraction Pattern (SADP) of this region is shown in Figure 9b. Although a small aperture was selected (10 μm, which illuminates a 1 μm diameter disc at the foil), a distinct ring pattern is observed indicating a microcrystalline structure. This ring pattern is typical of "transformed" bands.[6-10] The rings do appear somewhat broadened with the pattern indexing to be α—Fe(bcc). No fcc reflections or any individual carbide reflections can be seen.

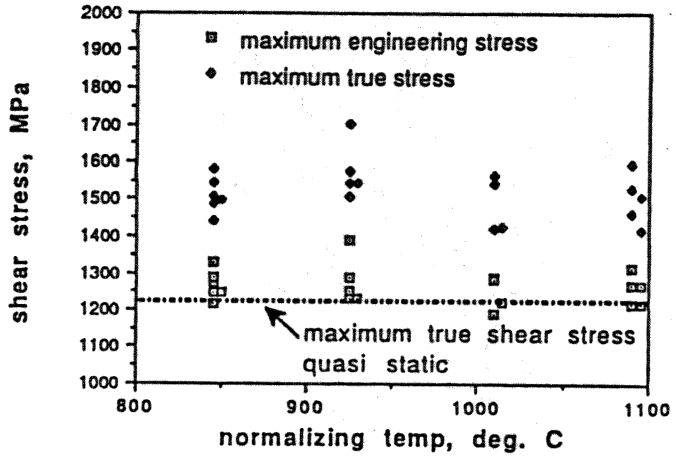

Figure 6. Maximum engineering shear stresses and true stresses versus normalizing temperature. Quasi-static data is from Cowie et al. (see References 1 and 2).

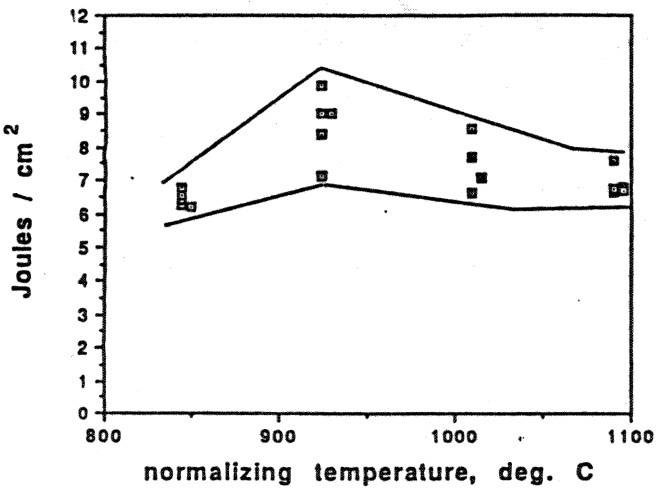

Figure 7. Energy absorbed to the point of instability per unit area sheared, E_i, versus normalizing temperature for a strain rate of $\dot{\gamma} = 10^5\ s^{-1}$.

6. GLENN, R. C., and LESLIE, W. C. Metall. Trans., v. 2, 1971, p. 29-54.
7. WINGROVE, A. L. *A Note on the Structure of Adiabatic Shear Bands in Steel.* Australian Defense Standard Laboratories, Technical Memo, 1971, p. 33.
8. WITTMAN, C. L., and MEYERS, M. A. *Effects on Metallurgical Parameters on Shear Band Formation in Low Carbon Steels.* To be published in Metall. Trans.
9. WITTMAN, C. L., MEYERS, M. A., and PAK, H. R. *Observation of an Adiabatic Shear Band in AISI 4340 Steel by High-Voltage Transmission Electron Microscopy.* Metall. Trans., v. 21A, March 1990, p. 707-716.
10. MEUNIER, Y., SANGOY, L., and PONT, G. *Metallurgical Aspects of Adiabatic Shear Phenomenon in Armor Steels with Perforation.* in Impact Loading and Dynamic Behavior of Materials. C. Y. Chiem, H. D. Kunze, L. W. Meyer, eds., DGM Information Gesellschatt, Oberursel/Frankfurt, v. 2:711, 1988.

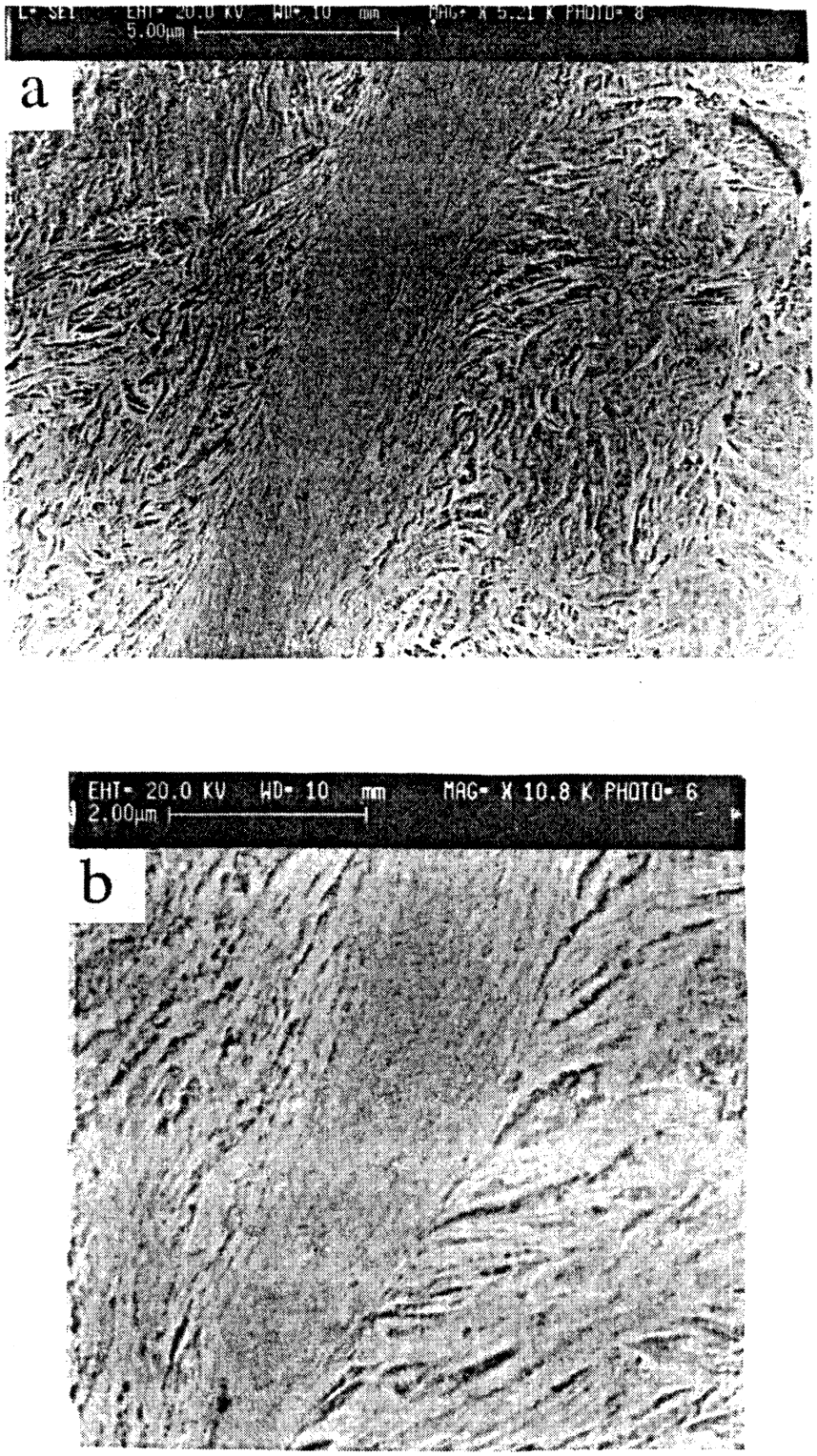

Figure 8. SEM of a shear band formed in a "hat" specimen.

Figure 9a. TEM bright field micrograph of shear band material in the N-925 microstructure.

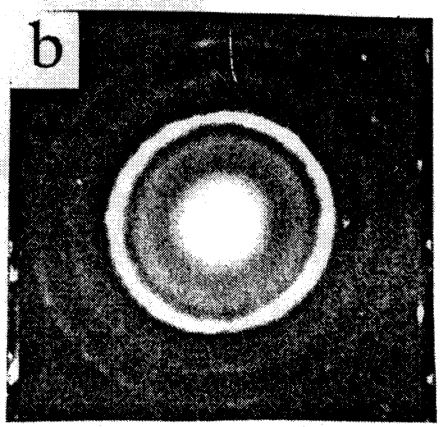

Figure 9b. SADP using a 10 μm aperture.

Using dark field microscopy and centering the first bright ring along the optical axis, the microcrystals can be individually illuminated. Figure 10 is such a dark field micrograph where the crystallite size can be determine to range from 8 nm to 20 nm. The change from true microcrystalline structure to "normal" heavily deformed martensite away from the band was gradual, agreeing with the works of Wittman et al.[8,9] SADPs as a function of distance away from the center of the band (see Figures 9b and 11a through 11d) illustrate the gradual transition from a ring pattern to a typical spot pattern.

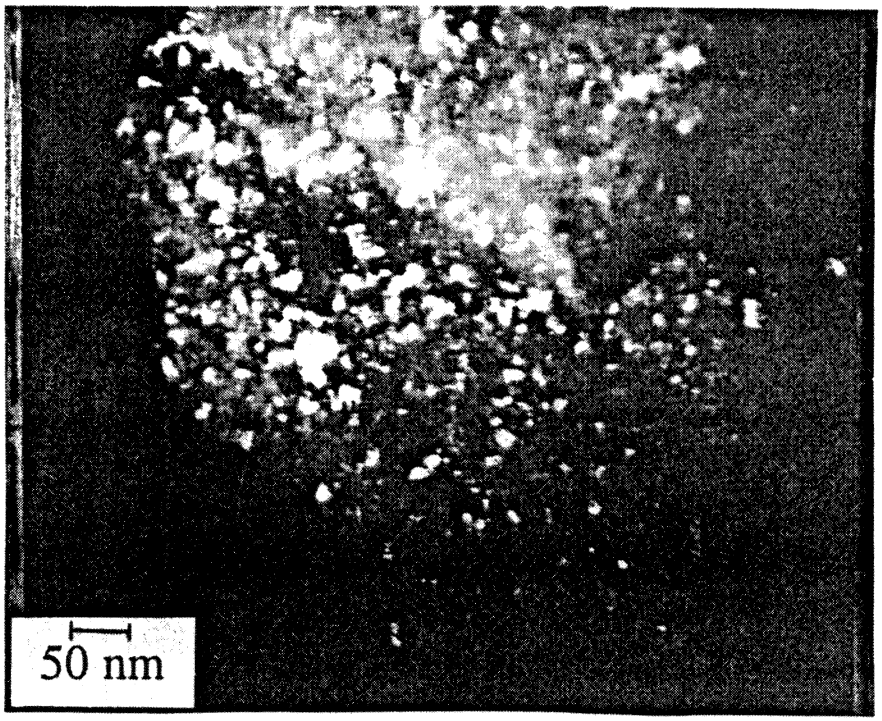

Figure 10. TEM dark field centering the first strong ring which illuminates the microcrystals. Sizes range from 8 nm to 20 nm in diameter.

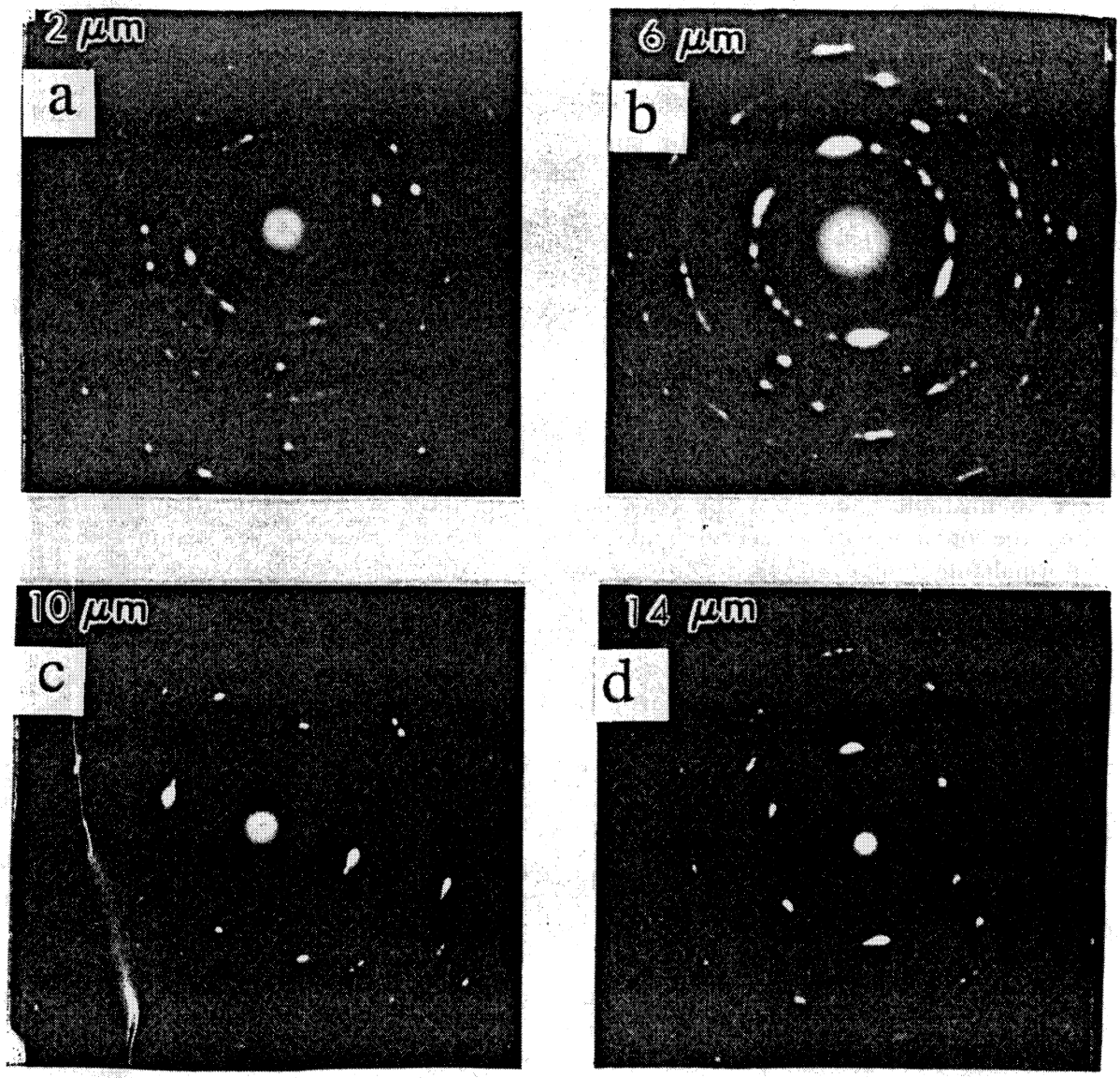

Figure 11. Variation of selected area diffraction patterns as a function of distance from the center of the shear band. Distance from the band center is noted on each pattern. Note the comparison to Figure 9b from near the center of the band.

DISCUSSION/CONCLUSIONS

The primary purpose of this paper is to examine for VAR 4340 steel at Rc52 the applicability of using the hat-shaped shear specimens to study shear band initiation mechanisms and present preliminary observations on their formation. The hat specimens with tailored stress-pulse profiles and controlled amounts of deformation produced unfractured specimens at various stages of shear band formation (prior to band formation, shear band propagation, and shear band widening). This technique provides a (simple) way to produce shear bands in a controlled manner at relatively high strain rates; thus, this method permits experimental correlation between metallurgical variables and shear band formation in high strength steels.

The relative resistance of the four microstructures to unstable shear at high strain rates is summarized in Figure 7. It shows that the influence of microstructure can be important in this regime of strain rates despite the intense heating that accompanies shear band formation. Since the principal variable which was studied, the carbide distribution, probably has little if any effect on the material behavior after destabilization, it must affect the processes leading to the destabilization of the deformation process. The fact that one condition had higher energy resistance even though all microstructures had equal hardness at this high strain rate is significant.

These same microstructures have been examined by Cowie et al.[1,2] at low to moderate strain rates. In their study, the 925°C normalizing treatment also produced a peak in the resistance to unstable shear, but the resistance to unstable shear had a minimum for 1010°C, suggesting the presence of a second peak in the instability strain at low strain rates for higher normalizing temperatures. Charpy tests over this same range of normalizing temperatures at room temperature and -40°C correlated in the same manner; two peaks in absorbed energy at room temperature, while the -40°C Charpy results showed a single peak in toughness. This suggests that the increase in strain rate in the "hat" shear tests is analogous to the decrease in temperature in the Charpy tests.

Examination by optical and electron microscopy of the hat specimens in various stages of shear band formation and propagation has not yet shown any significant difference between the four microstructures tested. The tips of the shear bands show the martensite laths gradually aligning with the shearing direction which agree with the observations of Wittman et al.[9] Note the absence of any observable grain structure within the shear band and the gradual change from the band to the matrix.

The TEM examination of the shear band showed the change from the internal shear band structure to the matrix structure to be gradual. This study has clearly resolved that the interior of the shear band has an extremely fine microcrystalline structure with grain diameters ranging from 8 nm to 20 nm. Previous studies had suggested that the crystallite size in "transformed" bands was between 100 nm to 1,000 nm.[10] However, this new evidence clearly shows that microcrystals exist in these shear bands, which are an order of magnitude smaller than this. This accounts for the difficult resolution of the band in earlier SEM and TEM studies. Foils that are many crystallites in thickness produce repeated scattering by subsequent crystallites and mask their true structure. No austenite or carbide reflections could be detected in the diffraction patterns taken from the regions showing the extremely fine microcrystals. Since a small crystallite size within the shear band would enhance the stability of austenite that was present, the complete absence of austenite reflections is significant.

It suggests that no transformation has occurred, and that the shear band is simply very heavily deformed martensite, in which both the extremely fine grain size combined with the additional carbon in solution (from dissolved carbides) have increased the hardness of the residual (after testing) microstructure. The absence of carbides combined with the microcrystalline structure would prevent preferential etching, creating the white etching typical of "transformed" bands.

ACKNOWLEDGMENTS

The work was performed at the University of California, San Diego (UCSD), and at the U.S. Army Materials Technology Laboratory, Watertown, MA. The work performed at UCSD was supported by the U.S. Army Research Office (ARO) under Contract No. DAAL-03-86-K-0169, as part of ARO's URI center for the Dynamic Performance of Materials. The authors are grateful to Mr. Jon Isaacs for valuable contributions in Hopkinson bar testing.

DISTRIBUTION LIST

No. of Copies	To
1	Office of the Under Secretary of Defense for Research and Engineering, The Pentagon, Washington, DC 20301
	Commander, U.S. Army Laboratory Command, 2800 Powder Mill Road, Adelphi, MD 20783-1145
1	ATTN: AMSLC-IM-TL
1	AMSLC-CT
	Commander, Defense Technical Information Center, Cameron Station, Building 5, 5010 Duke Street, Alexandria, VA 22304-6145
2	ATTN: DTIC-FDAC
1	Metals and Ceramics Information Center, Battelle Columbus Laboratories, 505 King Avenue, Columbus, OH 43201
	Commander, Army Research Office, P.O. Box 12211, Research Triangle Park, NC 27709-2211
1	ATTN: Information Processing Office
1	SLCRD-ZC, Kailasam Iyer
	Commander, U.S. Army Materiel Command, 5001 Eisenhower Avenue, Alexandria, VA 22333
1	ATTN: AMCLD
	Commander, U.S. Army Materiel Systems Analysis Activity, Aberdeen Proving Ground, MD 21005
1	ATTN: AMXSY-MP, H. Cohen
	Commander, U.S. Army Missile Command, Redstone Scientific Information Center, Redstone Arsenal, AL 35898-5241
1	ATTN: AMSMI-RD-CS-R/Doc
1	AMSMI-RLM
	Commander, U.S. Army Armament, Munitions and Chemical Command, Dover, NJ 07801
2	ATTN: Technical Library
1	AMDAR-LCA, Mr. Harry E. Pebly, Jr., PLASTEC, Director
	Commander, U.S. Army Natick Research, Development and Engineering Center, Natick, MA 01760-5010
1	ATTN: Technical Library
	Commander, U.S. Army Satellite Communications Agency, Fort Monmouth, NJ 07703
1	ATTN: Technical Document Center
	Commander, U.S. Army Tank-Automotive Command, Warren, MI 48397-5000
1	ATTN: AMSTA-ZSK
2	AMSTA-TSL, Technical Library
	Commander, White Sands Missile Range, NM 88002
1	ATTN: STEWS-WS-VT
	President, Airborne, Electronics and Special Warfare Board, Fort Bragg, NC 28307
1	ATTN: Library
	Director, U.S. Army Ballistic Research Laboratory, Aberdeen Proving Ground, MD 21005
1	ATTN: SLCBR-TSB-S (STINFO)
1	Fred J. Grace
	Commander, Dugway Proving Ground, Dugway, UT 84022
1	ATTN: Technical Library, Technical Information Division
	Commander, Harry Diamond Laboratories, 2800 Powder Mill Road, Adelphi, MD 20783
1	ATTN: Technical Information Office
	Director, Benet Weapons Laboratory, LCWSL, USA AMCCOM, Watervliet, NY 12189
1	ATTN: AMSMC-LCB-TL
1	AMSMC-LCB-R
1	AMSMC-LCB-RM
1	AMSMC-LCB-RP
	Commander, U.S. Army Foreign Science and Technology Center, 220 7th Street, N.E., Charlottesville, VA 22901-5396
3	ATTN: AIFRTC, Applied Technologies Branch, Gerald Schlesinger

No. of Copies	To
	Commander, U.S. Army Aeromedical Research Unit, P.O. Box 577, Fort Rucker, AL 36360
1	ATTN: Technical Library
	Commander, U.S. Army Aviation Systems Command, Aviation Research and Technology Activity, Aviation Applied Technology Directorate, Fort Eustis, VA 23604-5577
1	ATTN: SAVDL-E-MOS
	U.S. Army Aviation Training Library, Fort Rucker, AL 36360
1	ATTN: Building 5906-5907
	Commander, U.S. Army Agency for Aviation Safety, Fort Rucker, AL 36362
1	ATTN: Technical Library
	Commander, USACDC Air Defense Agency, Fort Bliss, TX 79916
1	ATTN: Technical Library
	Commander, U.S. Army Engineer School, Fort Belvoir, VA 22060
1	ATTN: Library
	Commander, U.S. Army Engineer Waterways Experiment Station, P. O. Box 631, Vicksburg, MS 39180
1	ATTN: Research Center Library
	Commandant, U.S. Army Quartermaster School, Fort Lee, VA 23801
1	ATTN: Quartermaster School Library
	Naval Research Laboratory, Washington, DC 20375
1	ATTN: Code 5830
2	Dr. G. R. Yoder - Code 6384
	Chief of Naval Research, Arlington, VA 22217
1	ATTN: Code 471
1	Edward J. Morrissey, WRDC/MLTE, Wright-Patterson Air Force, Base, OH 45433-6523
	Commander, U.S. Air Force Wright Research & Development Center, Wright-Patterson Air Force Base, OH 45433-6523
1	ATTN: WRDC/MLLP, M. Forney, Jr.
1	WRDC/MLBC, Mr. Stanley Schulman
	NASA - Marshall Space Flight Center, MSFC, AL 35812
1	ATTN: Mr. Paul Schuerer/EH01
	U.S. Department of Commerce, National Institute of Standards and Technology, Gaithersburg, MD 20899
1	ATTN: Stephen M. Hsu, Chief, Ceramics Division, Institute for Materials Science and Engineering
1	Committee on Marine Structures, Marine Board, National Research Council, 2101 Constitution Ave., N.W., Washington, DC 20418
1	Librarian, Materials Sciences Corporation, 930 Harvest Drive, Suite 300, Blue Bell, PA 19422
1	The Charles Stark Draper Laboratory, 68 Albany Street, Cambridge, MA 02139
	Wyman-Gordon Company, Worcester, MA 01601
1	ATTN: Technical Library
	Lockheed-Georgia Company, 86 South Cobb Drive, Marietta, GA 30063
1	ATTN: Materials and Processes Engineering Dept. 71-11, Zone 54
	General Dynamics, Convair Aerospace Division, P.O. Box 748, Fort Worth, TX 76101
1	ATTN: Mfg. Engineering Technical Library
	Worcester Polytechnic Institute, Mechanical Engineering Department, 100 Institute Road, Worcester, MA 01609
1	ATTN: Dr. R. Biederman
1	Dr. Isa Bar-On
1	Dr. F. Tuler
1	Dr. R. Sisson

No. of Copies	To
	Northwestern University, Department of Materials Science and Engineering, Evanston, IL 60208
2	ATTN: Dr. G. Olson
	Norton Company, Goddard Road, Northboro, MA 01532-1545
1	ATTN: K. Siebein
	U.S. Secret Service, 1310 L Street NW, Room 800, Washington, DC 20005
1	ATTN: T. Thomas
	Brown University, Box D, Providence, RI 02912
1	ATTN: Professor A. Needleman
1	Professor J. Duffy
1	Professor R. Clifton
1	Professor S. Nutt
	Colorado School of Mines, Metallurgical and Materials Engineering Department, Golden, CO 80401
1	ATTN: Professor G. Krauss
1	R. Weiss
	Carenter Technology Corporation, Tool and Alloy R&D, P.O. Box 14662, Reading, PA 19612 4662
1	ATTN: M. Schmidt
1	R. Hemphill
	Los Alamos National Laboratory, MS G730, Los Alamos, NM 87545
1	ATTN: M. Stevens
	University of California, San Diego, Department of Applied Mechanics and Engineering Sciences, La Jolla, CA 92093
2	ATTN: Professor S. Nemat-Nasser
2	Professor M. Meyers
1	Dr. Walter A. Backofen, Methodist Hill, Lebanon, NH 03766
	University of Dayton, Research Institute, Dayton, OH 45469
1	ATTN: Professor Stephen Bless
	California Institute of Technology, Seismological Laboratory 252-21, Pasadena, CA 91109
1	ATTN: T. Ahrens
	University of Virginia, Department of Materials Science, Charlottesville, VA 22901
1	ATTN: Professor G. Shiflet
	Director, U.S. Army Materials Technology Laboratory, Watertown, MA 02172-0001
2	ATTN: SLCMT-TML
4	Authors